Opto-Electronic Advances

Supplementary information

January 2023, Vol. 6, No. 1

DOI: 10.29026/oea.2023.210163

Carnivorous plants inspired shape-morphing slippery surfaces

Dong-Dong Han[1], Yong-Lai Zhang[1]*, Zhao-Di Chen[1], Ji-Chao Li[1], Jia-Nan Ma[1], Jiang-Wei Mao[1], Hao Zhou[1] and Hong-Bo Sun[2]

[1]State Key Laboratory of Integrated Optoelectronics, College of Electronic Science and Engineering, Jilin University, Changchun 130012, China; [2]State Key Laboratory of Precision Measurement Technology and Instruments, Department of Precision Instrument, Tsinghua University, Beijing 100084, China.

*Correspondence: YL Zhang, E-mail: yonglaizhang@jlu.edu.cn

This file includes:

Section 1: Materials
Section 2: Methods
Section 3: The detailed mechanisms for the performance improvement
Section 4: Supplementary figures
Section 5: Supplementary movies

Supplementary information for this paper is available at https://doi.org/10.29026/oea.2023.210163

Open Access This article is licensed under a Creative Commons Attribution 4.0 International License.
To view a copy of this license, visit http://creativecommons.org/licenses/by/4.0/.

© The Author(s) 2023. Published by Institute of Optics and Electronics, Chinese Academy of Sciences.

Section 1: Materials

Graphite was bought from Sigma-Aldrich. $NaNO_3$, H_2SO_4, $KMnO_4$, and H_2O_2 were purchased from Sinopharm Chemical Reagent. Deionized water (18.2 MΩ cm, 25 °C) was produced by using a water purification system (MILLIPORE). Membrane filters (0.22 μm in pore size) were bought from Shanghai Xinya water purifier factory. Oil was purchased from COFCO Group Co., Ltd. Fluorochrome was prepared according to the ref.[S1]. Plum juice was bought from Kangshifu Beverage Co., Ltd. Brandy was bought from Yantai Changyu Grape Wine Co., Ltd. Vinegar was bought from Shanxi shuita vinegar Co., Ltd. Soda water was purchased from Hangzhou Wahaha Group Co., Ltd. Beer was bought from Qingdao Lanbaoshi Jiuye Gufen Co., Ltd. Milk was bought from Ground Dairy Industry Co., Ltd.

Section 2: Methods

Preparation of graphene oxide (GO). GO was prepared via the Hummers method. 2 g of graphite powder, 2 g of $NaNO_3$, and 96 mL of concentrated H_2SO_4 (98%) were mixed at ≈0 °C. Then, 12 g of $KMnO_4$ was slowly added to the mixture at 0 °C for 90 minutes and kept at 35 °C for an additional 120 minutes. After that, 80 mL of distilled water was slowly added to the mixture. 10 mL of H_2O_2 (30%) was slowly dropped into the mix. Finally, GO aqueous solution was obtained by repeated washing with distilled water and high-speed centrifugation until the pH reached 7.

Preparation of waterproof oil-infused laser structured reduced GO/GO (oil-LRGO/GO) membranes. The GO membranes are fabricated by vacuum filtration. Afterward, the GO membranes are peeled from the membrane filter for further use. There is no further hydrophobic coating to the GO. The thickness of the GO membrane is ~20 μm; The roughness of the GO membrane surface is ~11 nm (root mean square); The Brunner-Emmet-Teller (BET) surface area (porosity) of the GO membrane is ~30 m^2/g. The brand of the femtosecond laser is LIGHT CONVERSION. The model of the femtosecond laser is PHAROS. Fs laser (λ=1030 nm, pulse duration=290 fs, repetition rate=200 kHz, laser fluence = 1.38 J/cm^2, Jicheng ultrafast equipment, Roban Nano system) is used to reduce GO and fabricate the Pitcher plants structure, forming an LRGO/GO bilayer structure. Due to the micro-nano structures of LRGO, the oil was fully infused into the structured LRGO layer by capillary force. Excess lubricant can be removed by vertical placement of the substrates for 1 hour. As a result, the oil-LRGO/GO membranes were prepared. The simple was cutting into desired shapes by a knife.

Characterization. The laser spot radius was measured using a laser scanning confocal microscope. Then the laser spot radius and measurement errors were analyzed by Origin software from the slope of the graph. Scanning electron microscope (SEM) images were obtained using a JEOL JSM7500 field-emission scanning electron microscope (FE-SEM). Confocal laser scanning microscope (CLSM) images were measured using a laser scanning confocal microscope (OLS4100). Raman spectroscopy was obtained using LabRAM HR Evolution. Fourier transform infrared (FTIR) spectroscopy was recorded using a Nicolet iS50 FT-IR spectrometer in the 2000–1000 cm^{-1} frequency range. X-ray photoelectron spectroscopy (XPS) was performed using an ESCALAB 250 spectrometer. The water contact angles (CAs) and sliding angles (SAs) were measured using a Contact Angle Meter SL200B (Solon Tech. Shanghai). Keithley 2635B was used to measure the electrical outputs.

Section 3: The detailed mechanisms for the performance improvement

The performance improvement can be explained by a classical model for bilayer beams[S2–S4].

$$\frac{1}{r} = \frac{6w_1w_2E_1E_2t_1t_2(t_1+t_2)(\alpha_1-\alpha_2)\Delta RH}{(w_1E_1t_1^2)^2+(w_2E_2t_2^2)^2+2w_1w_2E_1E_2t_1t_2(2t_1^2+3t_1t_2+2t_2^2)},$$

where, r: radius of curvature; 1: oil-LRGO, 2: GO; w: width; E: Young's modulus; t: thickness; α: moisture expansion coefficient; ΔRH, the difference in initial and final RH. The curvature is proportional to ΔRH. Greater $\Delta\alpha$ leads to much greater displacement.

Section 4: Supplementary figures

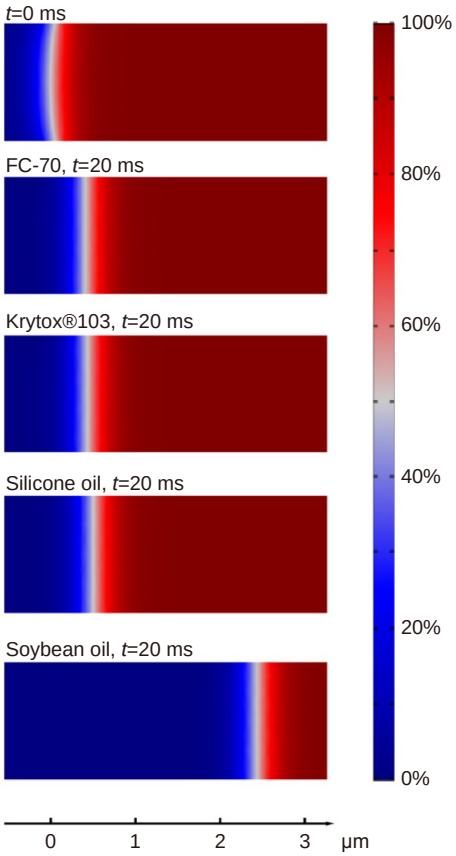

Fig. S1 | COMSOL simulation of the fluid mechanics on LRGO using different lubricants.

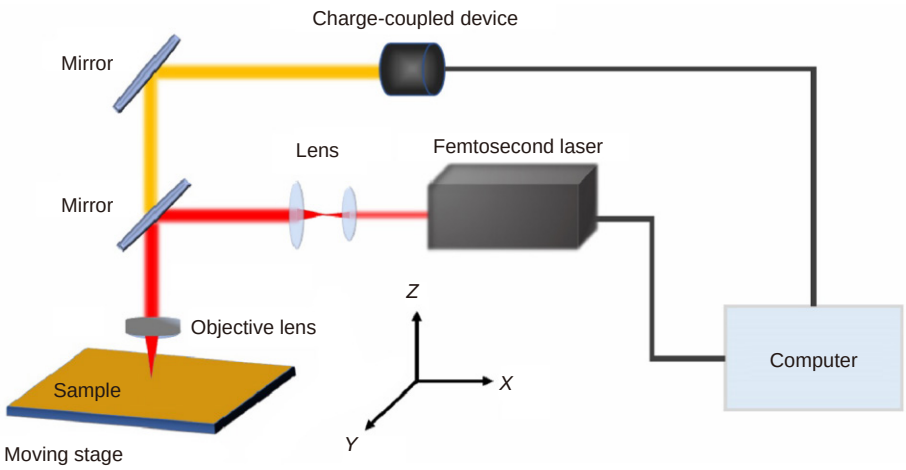

Fig. S2 | Schematic diagram for the direct laser writing system. The sample (GO membrane) was fixed on the moving stage. The femtosecond laser was focused on the GO surface, and the laser beam was scanned using the moving stages controlled by a computer.

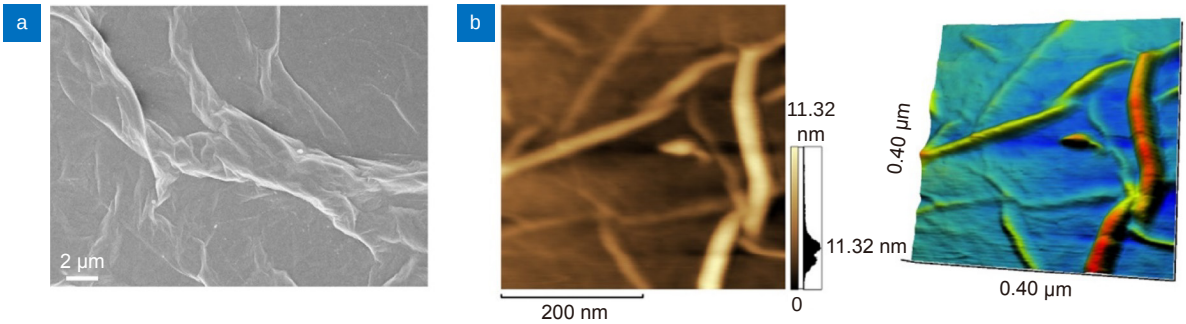

Fig. S3 | (**a**) SEM and (**b**) atomic force microscope images of the GO surface.

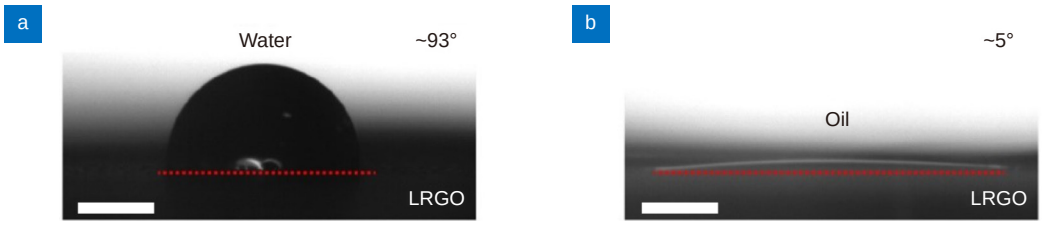

Fig. S4 | (**a**) Water and (**b**) oil contact angles on the LRGO surfaces. The scale bar is 1 mm.

Fig. S5 | The advancing and receding contact angles of oil-LRGO surface are 64° and 61°, respectively. The scale bar is 1 mm.

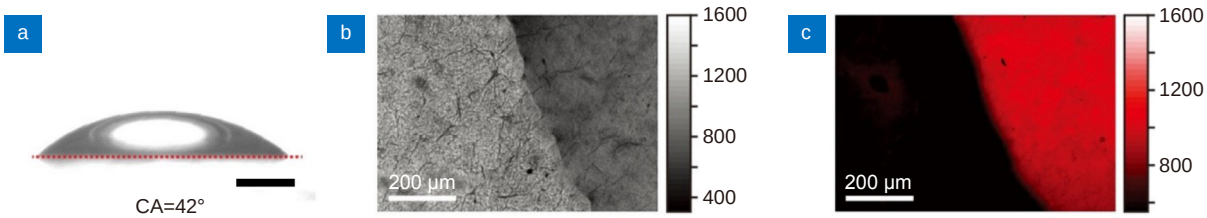

Fig. S6 | (**a**) CA of GO. The scale bar is 1 mm. (**b**, **c**)The fluorescence microscope images of GO surfaces after a water droplet containing fluorochrome sliding across.

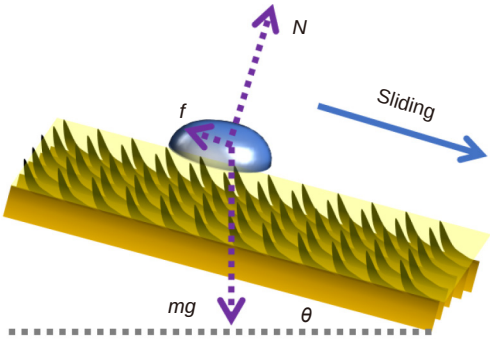

Fig. S7 | The schematic diagram for droplets sliding, representing the effect of gravity. The Furmidge equation could be used to describe the force balance: ref.[S5–S7]

$$mg\sin\alpha = \gamma_{LV}\, w(\cos\theta_R - \cos\theta_A)\ ,$$

where m, g, α, γ_{LV}, w, θ_R, θ_A are the weight, gravitational acceleration, sliding angle, surface tension, interfacial width of droplet, receding contact angles and advancing contact angles, respectively.

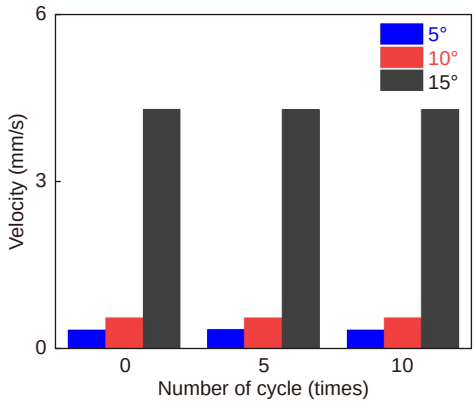

Fig. S8 | The long-term stabilities of droplet sliding performance on oil-infused LRGO surface with different titled angles.

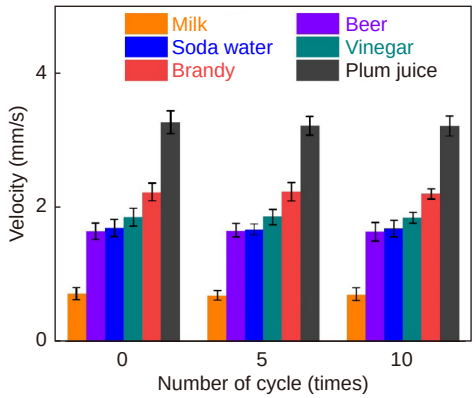

Fig. S9 | The long-term stabilities of the sliding performance of different liquid droplets on oil-infused LRGO surface.

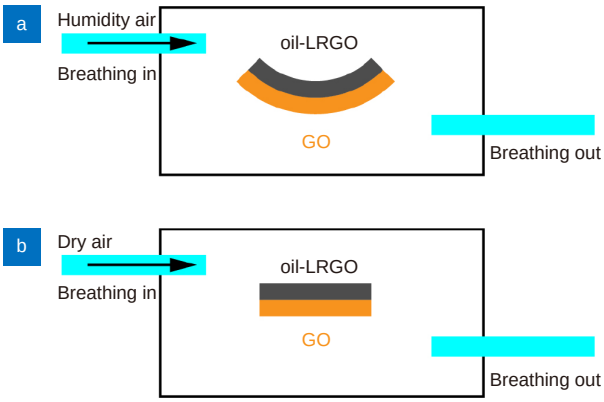

Fig. S10 | The schematic diagram for the moisture supplying system. (**a**) A pump was used to inject humidity air into the box. (**b**) Another pump was used to inject dry air into the box.

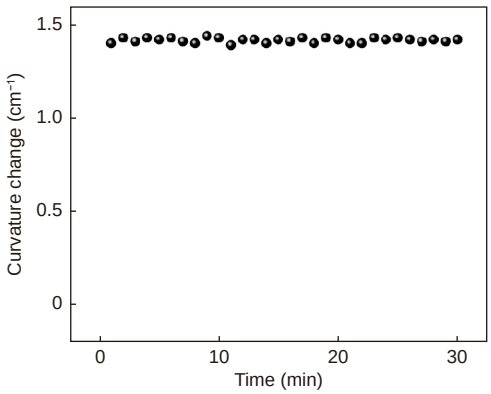

Fig. S11 | The bending curvature almost keeps a constant value after exposure to high moisture for 30 minutes.

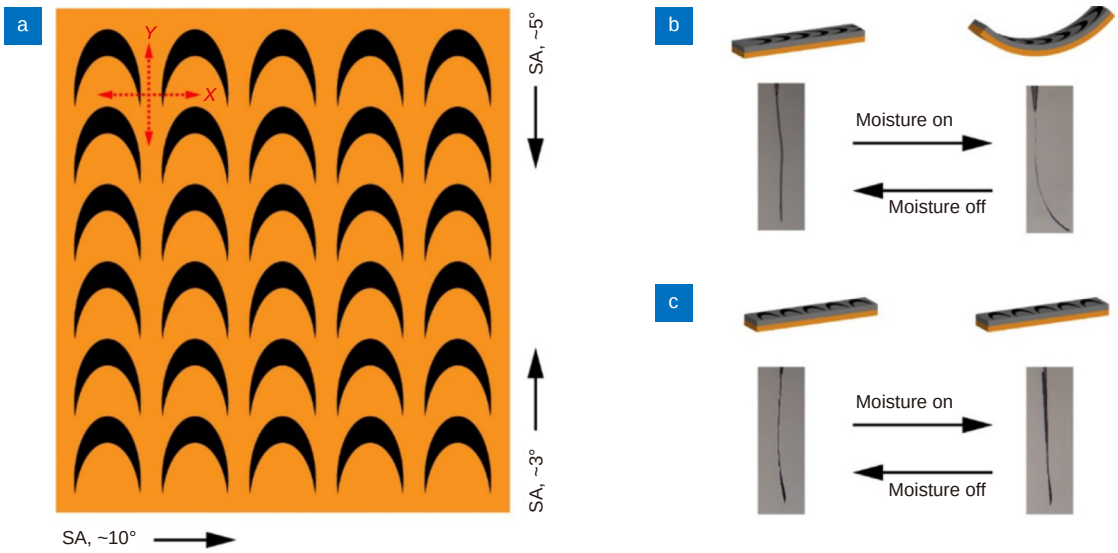

Fig. S12 | (**a**) The sliding angles of water on the liquid-infused surface in a different direction. (**b**, **c**) The anisotropic structure leads to anisotropic deformation under moisture actuation. The length of the ribbon is 12 mm.

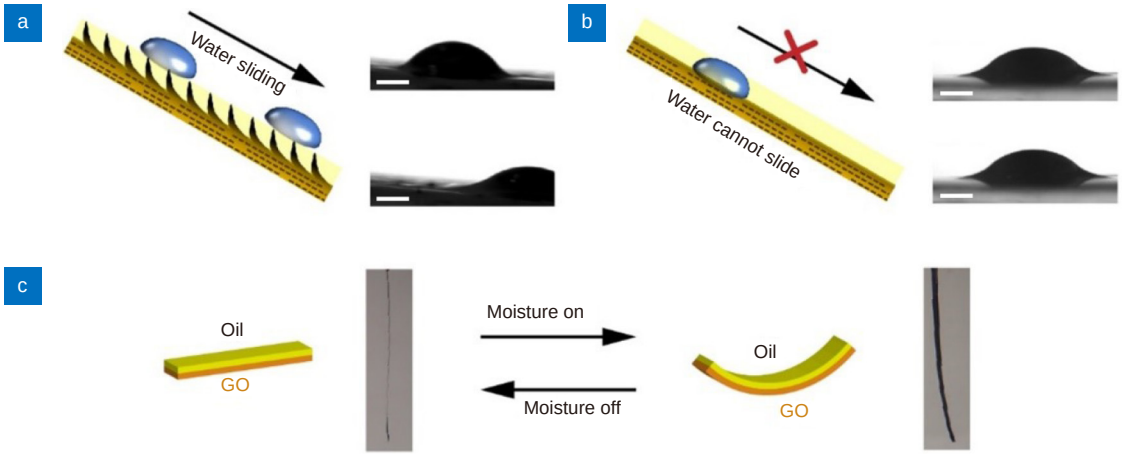

Fig. S13 | (**a**) Water droplets slide on the oil-LRGO surface because the LRGO is hydrophobic. The scale bar is 1 mm. (**b**) Water droplets cannot slide on the oil-GO surface because the GO is hydrophilic. The scale bar is 1 mm. (**c**) The oil/GO bilayer membrane occurs bending deformation under moisture actuation. The length of the ribbon is 12 mm.

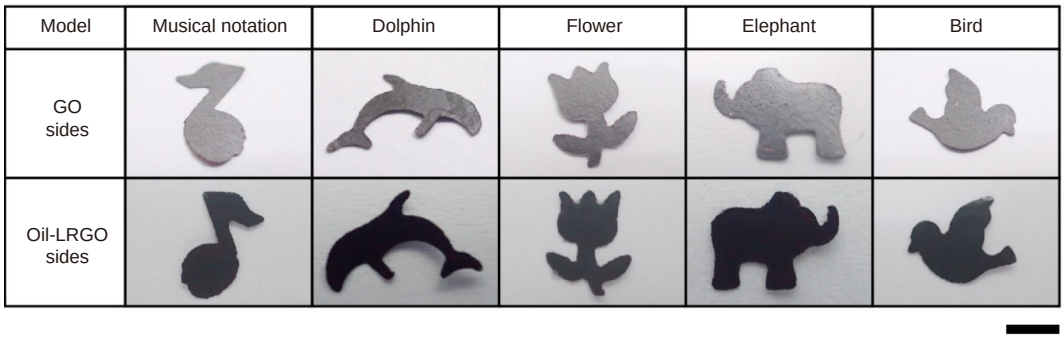

Fig. S14 | Different geometries of oil-LRGO/GO films prepared by artificial cutting techniques. The simple was cutting into desired shapes by a knife. The scale bar is 4 mm.

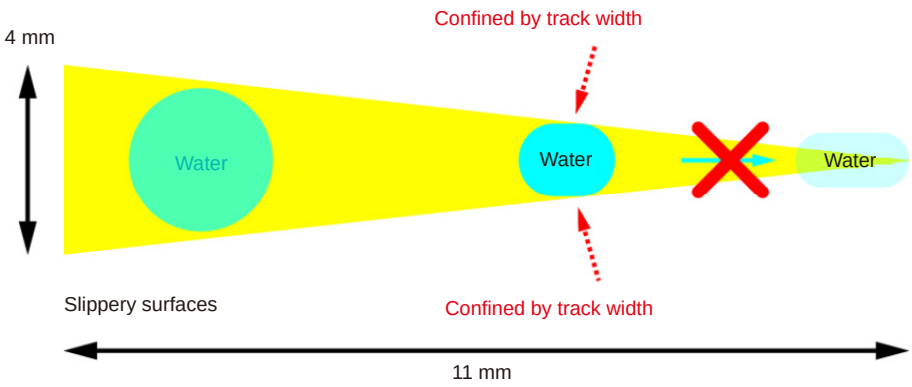

Fig. S15 | The schematic diagram for the droplets falling behavior shown in the Fig. 4(e).

Section 5: Supplementary movies

Movie S1. The sliding performance of a droplet on a tilted surface.

Movie S2. Droplet manipulation, including the active droplet catching and the passive droplet sliding.

References

S1. Sun K, Yang YK, Zhou H, Yin SY, Qin WP et al. Ultrabright polymer-dot transducer enabled wireless glucose monitoring *via* a smartphone. *ACS Nano* **12**, 5176–5184 (2018).

S2. Bi HC, Yin KB, Xie X, Zhou YL, Wan S et al. Microscopic bimetallic actuator based on a bilayer of graphene and graphene oxide. *Nanoscale* **5**, 9123–9128 (2013).

S3. Zang XN, Zhou Q, Chang J, Liu YM, Lin LW. Graphene and carbon nanotube (CNT) in MEMS/NEMS applications. *Microelectronic Eng* **132**, 192–206 (2015).

S4. Khan ZH, Kermany AR, Öchsner A, Iacopi F. Mechanical and electromechanical properties of graphene and their potential application in MEMS. *J Phys D Appl Phys* **50**, 053003 (2017).

S5. Furmidge CGL. Studies at phase interfaces. I. The sliding of liquid drops on solid surfaces and a theory for spray retention. *J Colloid Sci* **17**, 309–324 (1962).

S6. Dai XM, Stogin BB, Yang SK, Wong TS. Slippery wenzel state. *ACS Nano* **9**, 9260–9267 (2015).

S7. Zhang SN, Huang JY, Chen Z, Lai YK. Bioinspired special wettability surfaces: from fundamental research to water harvesting applications. *Small* **13**, 1602992 (2017).